Inline photothermal surface plasmon detector integrated in titanium dioxide waveguides

Andres Martinez[1], Vittorio Grimaldi[1], Christian De Vita[1], Deepak Kumar Sharma[2], Isabelle Gallet[2], Aurore Andrieux[2], Juan Arocas[2], Kamal Hammani[2], Laurent Markey[2], Jean-Claude Weeber[2], Alexandre Bouhelier[2], Marco Sampietro[1], Andrea Melloni[1], Francesco Morichetti[1]

Abstract— **Densely integrated photonic integrated circuits (PICs) require efficient solutions for monitoring the light intensity on chip in order to implement control and configuration operations to set and stabilize the working point of the circuit. To this end, waveguides supporting the propagation of surface plasmon polaritons (SPPs) are good candidates to realize small-footprint light detectors. In this work, we report on the realization of an in-line Surface Plasmon Detector (SPD) that exploits the photothermal effect to monitor the optical power in a titanium dioxide (TiO₂) optical waveguide. Detailed design guidelines are provided to maximize the responsivity of the SPD, taking into account the effects of the metal geometry on the coupling between the dielectric and plasmonic modes, the power dissipated in the metal, and the equivalent thermal resistance of the structure. Experimental validation of the proposed device is provided demonstrating an ultra-compact 1.6-μm-long SPD operating at a wavelength of 1550 nm with a sensitivity of – 20 dBm and a bandwidth higher than 100 kHz. The proposed device concept can be ported to generic dielectric platforms and to other wavelength ranges where SPP propagation is supported.**

Index Terms— **integrated photodetectors, integrated photonics, optical sensors, photothermal effects, surface plasmon polaritons.**

I. INTRODUCTION

Photonic Integrated Circuits (PICs) are evolving towards architectures with an ever-increasing scale of integration that implement more and more complex functionalities. To develop PICs that can be reconfigured reliably, on-chip photodetectors must be integrated to locally monitor the optical power and closed-loop control systems have to be designed to set and stabilize their working point. Semiconductor photodetectors are widely employed in the near-infrared range because of their small size, fast detection speed, high detection efficiency [1], and monolithic integration on silicon and III-V photonic platforms. This family of transducers includes photodiodes [2], photoconductors [3], sub-band-gap detectors based on defect state absorption [4], and surface state absorption [5]. However, these approaches cannot be directly deployed onto dielectric waveguide platforms, such as silicon (oxy) nitride or other glass-based technologies.

A. Martinez, C. De Vita, V. Grimaldi, M. Sampietro, A. Melloni, and F. Morichetti are with the Department of Electronics, Information and Bioengineering, University Politecnico di Milano, Piazza Leonardo da Vinci, 32, 20133, Milano, Italy. (email: francesco.morichetti@polimi.it).

D. K. Sharma, I. Gallet, A. Andrieux, J. Arocas, K. Hammani, L. Markey, J. Weeber, and A. Bouhelier are with Laboratoire Interdisciplinaire Carnot de Bourgogne CNRS UMR 6303, 9 avenue Alain Savary, Dijon, 21078, France

A promising approach to implementing light sensing in small-footprint devices is offered by surface plasmon polaritons (SPPs), which are guided waves that can propagate along the surface of a conductor [6] [7]. SPP waves remain tightly confined on the metal-dielectric interface because the free electrons of the conductor respond collectively by oscillating in resonance with the electromagnetic wave [7] [8]. SPPs are only possible for wavelengths longer than a particular critical wavelength, which depends on the plasma frequency and is specific to each metal [6] [7] [8]. Moreover, SPPs are only TM polarized as there is no solution to the Maxwell equations that would represent a bounded mode for the TE polarization [6]. As SPP propagation is associated with the absorption of optical power in the metal, a temperature-dependent change of the metal resistivity is generated by the photothermal effect, which can be exploited to monitor the intensity of the light in the waveguide [9] [10] [11] [12] [13]. Different configurations have been proposed for photothermal detectors such as a Wheatstone bridge [11] and hybrid plasmonic waveguides [10].

In this work, we demonstrate an in-line Surface Plasmon Detector (SPD) integrated into a TiO₂ platform that exploits the photothermal effect to monitor the optical power inside the waveguides. The device simply consists of a thin strip of gold placed underneath the TiO₂ core of the waveguide, whose light-dependent resistance is measured by using a four-probe lock-in detection scheme. The paper is organized as follows. In Sec. II we illustrate the working principle of the device and the design rules to optimize the device performance in terms of insertion loss and photothermal responsivity. To this end, systematic numerical simulations based on a multi-physics 3D finite element method (FEM) including optical, thermal, and electrical analysis were carried out to investigate the impact of the metal strip geometry in the coupling between the dielectric TiO₂ waveguide and the SPP waveguide, and to maximize the absorption efficiency in the metal. In Sec. III the technology employed to integrate the SPD on a TiO₂ platform is described. Experimental results reported in Sec. IV demonstrate the functionality of the device both in terms of responsivity (-20 dBm) and speed (> 100 kHz). A concluding section summarizes the main achievement of this work.

II. DEVICE CONCEPT AND DESIGN OPTIMIZATION

The waveguide used for this work is realized with an air-cladded 1.2 μm-wide and 370 nm-high titanium dioxide (TiO₂) core on top of a 2 μm-thick silicon dioxide (SiO₂) on a Si substrate. In the SPD region, a gold strip is inserted underneath the waveguide core, as shown in Fig. 1(a) and (b). At the transition between the dielectric waveguide (no metal strip) and the plasmonic waveguide, the TM fundamental mode of the

dielectric waveguide may excite several SPP modes (see Fig. 2) [6] [14] [15]. SPP modes propagate in the plasmonic waveguide with different phase constants and accumulate different phase shifts for the same travelled distance. At the end of the metal strip, the relative phase between the SPPs modes modifies the shape of the overall electromagnetic field and hence the mode matching with the fundamental TM mode of the output dielectric waveguide. This constructive (maximal transmission) or destructive (minimal transmission) interference results in an insertion loss that depends on the metal strip length L.
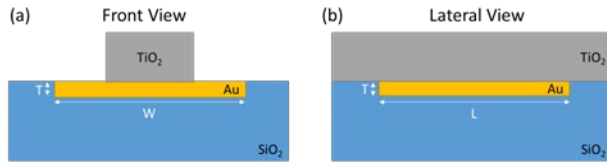

Fig. 1. Front (a) and lateral (b) view of the platform with the SPD. The width and thickness of the TiO$_2$ core are 1.2 μm and 370 nm, respectively. A thin strip of gold is realized below the TiO$_2$ core with thickness T, width W, and length L, which are the SPD parameters optimized by numerical simulations.
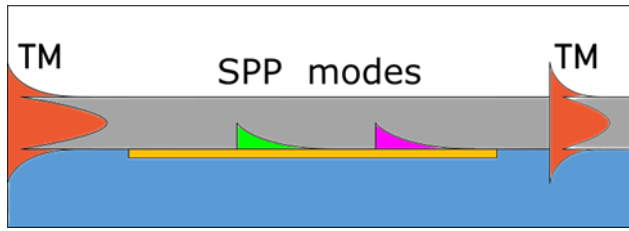

Fig. 2. Propagation of a surface plasmon excited by a TM dielectric mode. When the TM mode encounters the metal strip (yellow), it may excite several SPP modes (indicated with different colors) that propagate at different phase velocities and interfere constructively or destructively at the end of the plasmonic waveguide depending on the strip length L.

In the next sections, 3D FEM Multiphysics simulations are reported to analyze and optimize the coupling between the dielectric and the plasmonic modes. Factors such as the power dissipated inside the metal and the thermal behavior of the whole structure are investigated to maximize the responsivity of the device while keeping a low insertion loss for in-line detection of the guided light. All the reported simulations are carried out at a wavelength of 1550 nm.

A. OPTICAL ANALYSIS

The design of the in-line SPD detector has to be optimized in order to maximize the optical power absorption in the metal strip (this being at the origin of the photothermal effect), while keeping low the overall loss, meaning that other sources of loss (e.g., out of plane scattering and back reflections) must be minimized. To this end, full vectorial EM simulations were carried out to evaluate the dependence of the complex refractive index of the SPP modes on the transversal geometry of the metal strip. The refractive indices of the SiO$_2$ bottom oxide and the TiO$_2$ layer are 1.445 and 2.2, respectively, as confirmed by material characterization (see Sec. III). The cross-sectional shape of the fundamental mode of the SPP waveguide (TM-polarized) is shown in Fig. 3(a). The waveguide supports the

propagation of higher order modes, as the one shown in Fig. 3(b), whose effects will be studied in the following.
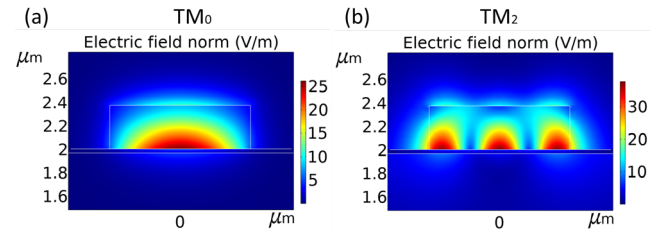

Fig. 3. Electric field profile of the guided modes of the plasmonic waveguide with T = 34 nm and W = 3 mm: (a) first order TM$_0$ and (b) third order TM$_2$ SPP modes. The second-order mode (not shown) is not excited by the TM mode of the input dielectric waveguide and does not contribute to the photo-thermal response of the device.

Figure 4(a) shows the real part (solid blue line) and the imaginary part (solid orange line) of the effective index of the fundamental mode versus the thickness T of the metal strip. The propagation loss

$$\alpha = -\frac{4\pi \, \Im[n_{eff}]}{\ln(10) \, \lambda_0} 10^{-5} \ [\text{dB/μm}], \tag{1}$$

which depends on the field intensity adjacent to the Au strip, increases for thinner strips. For thick strips, the evanescent component of the field penetrates more into the metal [16], but the rapidly decaying SPP mode profile makes this contribution too small to affect the propagation loss α. Furthermore, if the metal is too thick, the significant discontinuity at the edges of the metal strip would severely increase back reflections and reduce the light coupling to the detector. Thus, for light monitoring applications, the metal thickness should be maintained thin enough to increase the gold absorptance while also minimizing back reflection loss. In the following, a thickness $T = 34$ nm is assumed. Also, we observe a decrease in both the real and the imaginary (absolute value) part of the refractive index versus the thickness of the gold. This behavior is typical of a short-range surface plasmon polariton [6]. The large index contrast between the dielectric (2.2 for the TiO$_2$ and 1.445 for the SiO$_2$) introduces a larger cutoff frequency for the long-range modes, which in the considered structure are not supported [17].

Concerning the cross-sectional width W, the gold strip should be as narrow as possible to maximize the SPD responsivity. In this way, the equivalent thermal resistance of the detector increases, inducing a larger variation of the temperature and consequently of the read-out voltage (see Sec. B) for the same amount of dissipated power. Since the lateral confinement of the SPP modes is given by the width of the dielectric core (that in the considered case is 1.2 μm), there is a minimum width W_{min} of the metal strip for which the guided light does not interact with the free electrons of the gold strip outside the core. As shown in Fig. 4(b), this implies that real (solid blue line) and imaginary (solid red line) parts of the effective index n_{eff} of the SPP mode remain constant for $W > W_{min}$. Choosing a strip width slightly wider than W_{min} guarantees the highest responsivity while keeping the detector robust to fabrication tolerances. For the considered structure, $W_{min} = 2.6$ μm, so W was set to 3 μm.
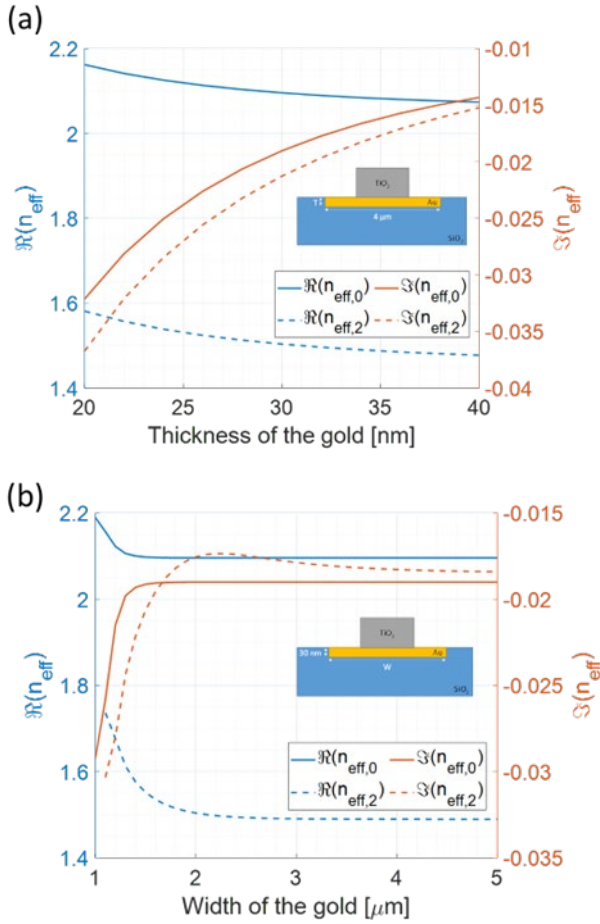
Fig. 4. (a) Real (blue) and imaginary (orange) parts of the SPP modes refractive index versus the thickness T of the gold strip. (b) Real (blue) and imaginary (orange) parts of the SPP modes refractive index vs gold width.

The length of the metal strip L is the fundamental design parameter as it determines the intensity of the transmitted optical wave and the amount of optical power that is absorbed by the metal. Fig. 5 shows the simulated normalized transmittance P_{out} across the SPP detector versus the length L ($W = 3$ μm and $T = 34$ nm). Results show that the TM transmission has a decaying sinusoidal behavior with a period of 2.4 μm. The exponential decay is due to the fact that the SPD has a fundamental mode with a complex-refractive index $n_{eff} = 2.084 - i0.016$ which corresponds to a propagation loss of 0.56 dB/μm. The periodic oscillation suggests that another SPP mode is excited, which propagates independently along the top and bottom surfaces of the metal at a different speed. Numerical simulations show that the waveguide supports the propagation of three SPP modes. In Fig. 3(b) we show the electric field profile of the third mode, whose complex effective index is shown in Figs 4(a) and (b) in dashed lines. The second mode is not shown because its electric field has an odd symmetry in the horizontal direction and it is not excited by the fundamental TM mode of the dielectric waveguide. The real part of the refractive index of the first and third modes is substantially different, this meaning that the two modes travel with a different phase velocity and accumulate a relative phase shift along the SPP waveguide. When the relative phase difference between the two SPP modes is a multiple of 2π, the overlap with the fundamental

TM mode of the output dielectric waveguide is maximized and P_{out} is maximum. The beat length ΔL is related to the difference between the real part effective index of the two SPP modes as

$$\Delta L = \frac{\lambda_0}{\Re\{n_{eff,0}\} - \Re\{n_{eff,2}\}} \qquad (2)$$

In the considered SPP waveguide geometry ($W = 3$ μm and $T = 34$ nm), where $\Re\{n_{eff,0}\} = 2.084$ and $\Re\{n_{eff,2}\} = 1.489$, a beat length $\Delta L = 2.6$ μm is found, which is in very good agreement with the result shown in Fig. 5. The minima in the transmitted power of Fig. 5 occur when the two interfering SPP modes are out of phase at the end of the metal strip. Since the transmittance is almost zero in all the minima (thus corresponding to complete destructive interference), we can conclude that the two modes are excited with a similar efficiency at the transition between the dielectric and the SPP waveguide and that they have a similar propagation loss along the SPP waveguide, as confirmed by the value of the imaginary part of the refractive index shown in red dashed lines in Fig. 4(a) and (b). From these figures it can also be appreciated that the difference between the real part of the effective index of the two SPP modes is almost independent of the thickness of the gold strip T and the width W (at least for $W > 3$ μm); this means that the beat length ΔL is not critically affected by fabrication tolerances. Moreover, the beat length does not change significantly with wavelength: Fig. 6 shows that the refractive index difference $\Delta\Re\{n_{eff}\} = \Re\{n_{eff,0}\} - \Re\{n_{eff,2}\}$ between the two SPP modes changes by only ± 4% across a wavelength range of more than 60 nm, thus enabling the SPD to work on a broad wavelength range.
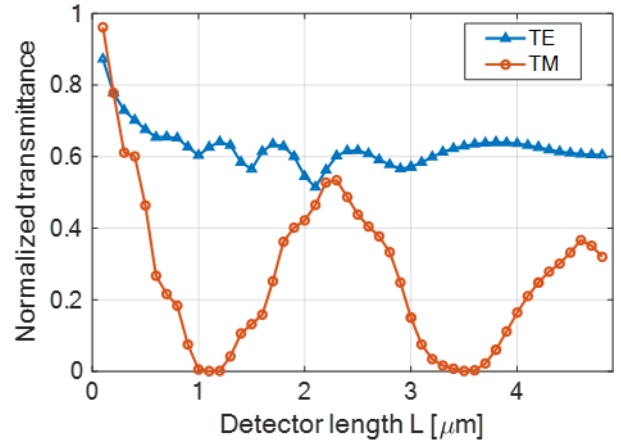

Fig. 5. Normalized transmittance through the SPD versus the metal strip length L for TE (blue) and TM (orange) input modes. The width and thickness of the strip are $W = 3$ μm and $T = 34$ nm.

This beating effect disappears for TE propagation, where SPP modes cannot be excited; in this case, P_{out} simply shows an exponential decay due to absorption in the metal strip. The shallow fluctuations on top of both TM and TE curves, with a period of about 500 nm, depend on Fabry-Perot (FP) cavity effects due to internal back reflections at the metal-dielectric interface; as the detector length L increases, this FP effect reduces because of the increased cavity loss due to metal absorption. As a result, the TE transmittance flattens after about 3 μm, while the TM mode maintains the beating effects between the two SPP modes.
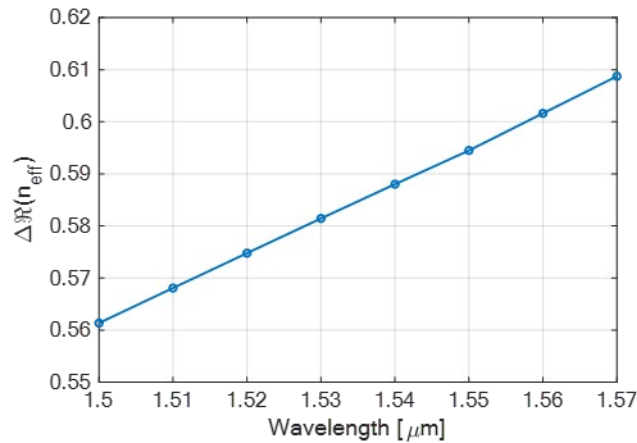
Fig. 6. Simulation of the difference between the real part of the effective refractive index of the first SPP mode (blue) versus wavelength. The simulation suggests that the difference between the real part of the modes remains constant over a large bandwidth.

Numerical simulations were carried out to localize optical absorption across the waveguide. Since TiO$_2$ is assumed to be fully transparent in the considered wavelength range (1550 nm), power dissipation occurs only within the Au layer. More in detail, in the cross-sectional plane the dissipated power is mostly concentrated within two-thirds of the core width [Fig. 7(a)], while it longitudinally spreads all along the detector, with a maximum dissipation at its center [Fig. 7(b)].

The absorption efficiency

$$\eta = \frac{P_d}{P_{loss}}, \quad (3)$$

which is defined as the ratio between the power dissipated in the gold P_d and the overall losses P_{loss}, gives a direct measurement of the capacity of the gold to transform the lost power into heat. Note that P_{loss} includes the loss due to radiated light and back reflection due to mode mismatch at the input and output sections of the SPP waveguide. In Fig. 7(c), the simulated losses efficiency is shown, highlighting how the absorption of the TM mode (orange) exhibits both the oscillations mentioned previously: the fast fluctuations due to the Fabry-Perot cavity are superimposed on the wide oscillations due to the coupling of the SPP propagating modes. For short lengths, P_{loss} is dominated by the coupling mismatch and η is only about 10%. As the length increases the coupling losses remain constant but P_d increases and so does η. An efficiency of 42.5% is achieved for the TM mode at $L = 2.3$ μm. Notably in this working point, η is 1.7 times bigger than the value observed for TE propagation (about 25%), demonstrating the benefit of SPP propagation. The absorption efficiency increases up to 50.4% at $L = 4.7$ μm, which coincides with the second transmittance peak. This is a remarkable result since there are lengths for which the transmitted optical power and gold absorptance are maximum. The absorption efficiency is limited by the coupling losses and the mismatch between the waveguide mode and the SPPs modes, and it can be further improved by introducing a mode adapter at the input/output sections of the plasmonic waveguide.
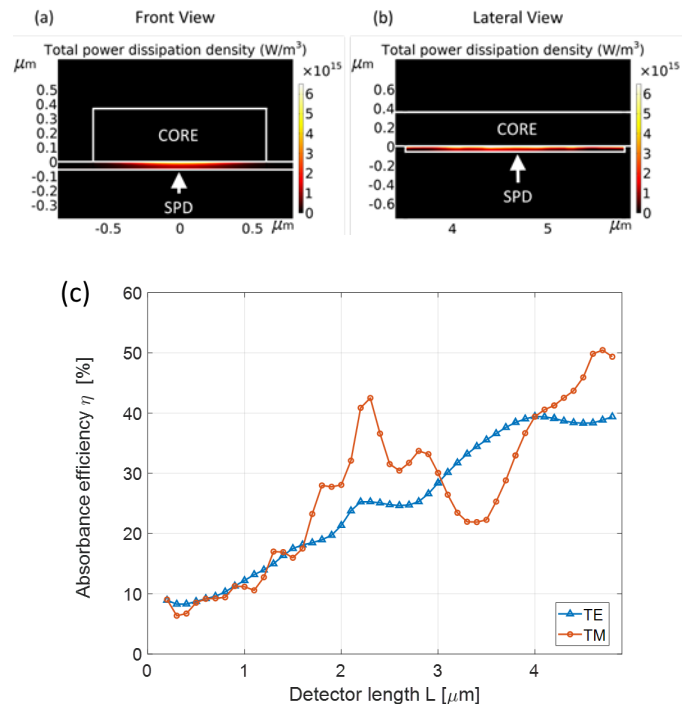

Fig. 7. Front (a) and lateral (b) view of the simulated power dissipated density. (c) Absorbance efficiency η, defined as the ratio between the power dissipated in the gold strip and the overall loss of the SPD versus the detector length L for TE (blue) and TM (orange) modes.
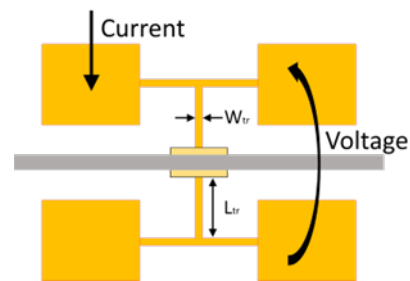

Fig. 8. Schematic of the SPD.

B. THERMO-ELECTRICAL ANALYSIS

In the proposed photothermal detector, the optical power dissipated by the metal of the SPP waveguide causes a temperature variation that induces the bolometric effect [10]. By measuring the change of the voltage drop due to the variation of the metal's resistance, it is possible to measure the optical power in the waveguide.

Figure 8 shows a top-view schematic of the complete device. The metal structure of the SPD is designed in order to enable the measurement of the light-induced temperature variation of the metal strip by means of a 4-probe technique. A small current I_s is forced between the two pads on the left, while a light-dependent voltage change ΔV is measured with a high-impedance amplifier across the two pads on the right. The 4-probes measurement allows to minimize the effect of the parasitic series resistance of the bonding wires and pads. Furthermore, a lock-in readout scheme is preferred for the readout, allowing to minimize the contribution of the 1/f noise

of the preamplifier, maximizing in this way the sensitivity of the power monitor. For the design optimization of the electronic access to the detector, we varied the width of the sensing track W_{tr} from 200 nm to 1600 nm. A narrow width W_{tr} increases the equivalent thermal resistance from the plasmonic waveguide to the contact pads in such a way that, even though gold is a good thermal conductor, heat does not spread through the sensing tracks and remains mostly localized around the waveguide. Therefore, the smaller W_{tr}, the larger is the thermal resistance R_{th}, and hence the temperature variation. The temperature profile along the detector is presented in Fig. 9 for an input TM mode with a power P_{in} = 1 mW, reference room temperature (that is 25°C for P_{in} = 0). We considered two different lengths L of the detector and two different widths of the arms W_{tr}. For W_{tr} = 200 nm and L = 1.6 µm, we obtain a peak around 40°C, which is 15 °C higher than room temperature. These results also provide an optimal length for the sensing tracks as no temperature variation is observed after 10 µm (W_{tr} = 200 nm) or 20 µm (W_{tr} = 1600 nm).
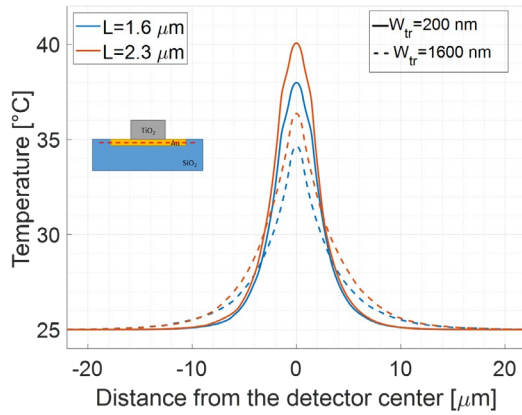

Fig. 9. Transversal SPD temperature profile for an input power P_{in} = 1 mW.

The thermoelectric performance of the proposed plasmonic detector is characterized by its responsivity R_d, defined as

$$R_d = \frac{\Delta V}{P_d}, \tag{4}$$

where ΔV is the voltage difference observed when a current I_s is forced through the circuit, and

$$\Delta V = I_s \, \Delta R = I_s \, R_0 \, \alpha \, \Delta T, \tag{5}$$

where R_0 is the resistance of the detector at reference room temperature and α is the temperature coefficient of the resistance of the gold.

Figure 10 shows the simulated voltage variation ΔV versus the optical power P_{in} at the input section of the detector. A temperature coefficient resistance α = 3.4·10⁻³ [1/K] is considered. Simulations are performed when I_s = 25 µA for W_{tr} = 200 nm (solid lines) and 1600 nm (dashed lines), and L = 1.6 µm (blue) and 2.3 µm (orange). Since the temperature varies linearly with P_{in}, and the resistivity varies linearly with temperature, ΔV is directly proportional to P_{in}. The voltage variation is very sensitive to the track width, for which we have

a factor of 5 between the slope of the curves with W_{tr} = 200 nm and 1600 nm; much less sensitivity is observed versus the detector length L, where the slope change is less than 15%. This behavior is due to the fact that the total electrical resistance is dominated by W_{tr} rather than by L. Since the absorbed optical power P_d increases with L, the best detector is not that with the smallest footprint, but that with the best compromise between the absorption efficiency η and the total electrical resistance, which is L = 2.3 µm and W_{tr} = 200 nm.
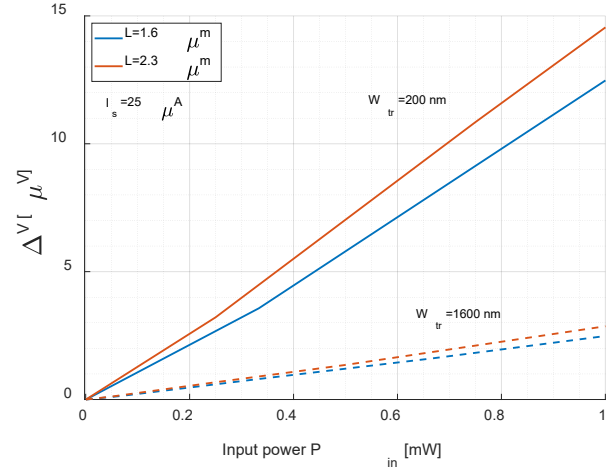

Fig. 10. Simulated variation of the voltage drop across the SPD for increasing power in the waveguide P_{in} for I_s = 25 µA. The detectors with W_{tr} = 200 nm perform around 5 times better than the ones with W_{tr} = 1600 nm. Fixing the width of the tracks, the longer detector performs better, given the longer absorbing region.

III. TECHNOLOGY AND DEVICE FABRICATION

All devices are fabricated on a 22 mm by 22 mm silicon chip covered by a 2 µm thick thermally grown SiO_2 layer. The devices are produced by three consecutive steps of electron-beam lithography. In the first step, the plasmonic gold detectors and their 4-probe addressing electrodes are patterned in a double-layer of PMMA (poly(methyl methacrylate)). This initial step is finalized by subsequent evaporation of a 3 nm Cr layer and a sub-40 nm Au film followed by a lift-off process. A 370 nm polycrystalline anatase TiO_2 layer is then deposited on the entire chip by electron-beam evaporation of a suitable target material on a sample holder maintained at 470 °C. Ellipsometry of this layer gives a refractive index of 2.2 at 1550 nm. The TiO_2 PIC [18] including waveguides and grating couplers is patterned in a second electron-beam lithography step in a negative tone resist which is then used as a hard mask during the following inductively coupled plasma reactive ion etching (ICP-RIE) of the TiO_2 layer. Here, we use a CF_4 plasma (20sccm) with a radiofrequency power of 50W, and an ICP power of 200 W, under a pressure of 4.5 mTorr at 0 °C to etch the layer. The last electron-beam lithography step consists of realizing macroscopic pads for electrically contacting the device with an external control and measurement electronics. The pads are made of 10 nm thick Cr and 200 nm thick Au layers to insure mechanical robustness against wire bonding. The TiO_2 waveguides are 1200 nm-wide, 370 nm-high and 1.5 mm-long. A portion of such a waveguide and a dummy Au detector (without the sensing tracks) are shown in Fig. 11(a). In

this example, the length L of the detector placed under the waveguide is 1.6 µm by a width W of 3 µm. Figure 11(b) shows an overview of a detector fully connected to its four-probe electrode systems.
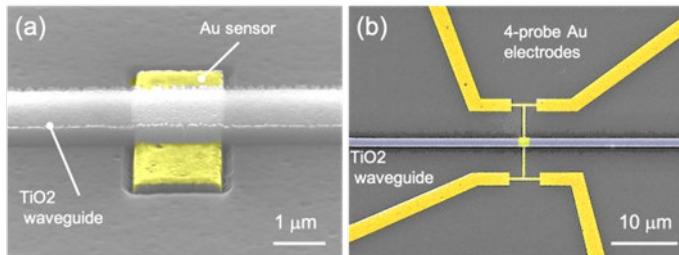

Fig. 11. False color SEM photographs of the TiO₂ testing PICs. (a) Dummy detector L = 1.6 µm and W = 3 µm placed underneath a TiO₂ waveguide. (b) overview of the SPD and its addressing electrodes arranged in a 4-probe configuration. The yellow hue highlights the Au parts of the device.

IV. EXPERIMENTAL RESULTS

Light coupling into the chip was achieved by using vertically emitting grating couplers designed to operate on TM polarization. Straight waveguides integrating SPDs with increasing length L were fabricated to assess the insertion loss (IL) and the back reflections of the SPD. Fig. 12 shows the transmitted optical power P_{tx} versus L normalized to a reference all-dielectric waveguide (L= 0). Experimental data are averaged over a wavelength range from 1520 nm to 1580 nm, where the SPDs exhibit a flat spectral response, and the error bars indicate the standard deviation evaluated on several nominal identical samples. A very good agreement is found with numerical simulations (data from Fig. 5 are reported in dB-scale for a direct comparison) on the position of the minimum transmission (around 1.1 µm) and the maximum transmission (2.2 µm). The insertion loss in the transmission maxima (5.5 dB) is higher than the value expected from simulations (2.5 dB); we believe that this is caused by some scattering loss in the plasmonic waveguide due to surface roughness at the metal-dielectric interface. The back reflection of each SPD was measured by using coherent optical frequency domain reflectometry [19] and amounts to –17 (± 0.7) dB, in agreement with electromagnetic simulations. This means that mode adapters from the dielectric to the plasmonic waveguide are not necessary, even though they could reduce the scattering loss.

Fig. 13 shows the light-dependent change of the voltage ΔV across the SPD, as measured by a lock-in scheme, for increasing power P_{in} in the waveguide, when a current I_s = 25 µA is applied. I_s is constant and does not change when light travels through the waveguide, nor when the optical power gets dissipated in the gold. Also, being 25 µA and the optical power inside the WG > -20 dBm, the dissipated power due to the light is 2 orders of magnitude higher than that due to I_s. For these reasons, any possible thermal effect caused by I_s is negligible. In agreement with the numerical results of Fig. 10, ΔV increases linearly versus P_{in}. The responsivity R_d, which is given by the slope of the linear fit (red), is equal to 7.5 µV/mW in good agreement with simulations of Fig. 10. With the lock-in

amplifier bandwidth set to 1 Hz, the minimum detectable power is about -20 dBm, which corresponds to a voltage change ΔV = 75 nV, that is induced by a temperature increase by only 1.75e-3 °C. The detector sensitivity can be extended to lower optical power by increasing I_s, the limit being given by the current handling capability of the thin arms of the detector, which in our case is about 250 µA. With this supply current we were able to measure a minimum optical power of -30 dBm in the waveguide. In the considered device the dynamic range is restricted to 15 dB by the maximum power in the waveguide (P_{in} = 0.75 mW), which is limited by the coupling efficiency of the grating couplers (13 dB loss each).
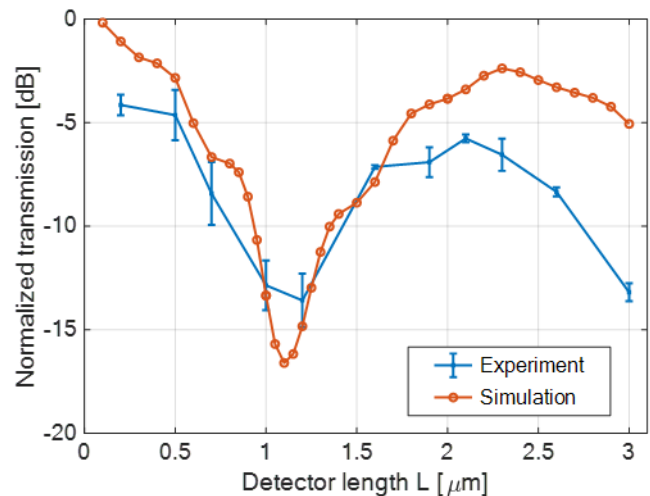
Fig. 12. Normalized transmitted power vs. SPD length for TM mode. The experimental curve (blue) is in good agreement with FEM simulation (orange).

Fig. 13. Measured responsivity of the SPD for I_s = 25 µA. The voltage is linear w.r.t the optical power and the responsivity equals 7.5 µV/mW

The time response of the SPD is shown in Fig. 14. It was measured by modulating the input light with a square wave at 20 kHz and reading the detector voltage ΔV with an

oscilloscope triggered by the modulating signal. The time constant of the detector response (red curve), which is defined as the time it takes for th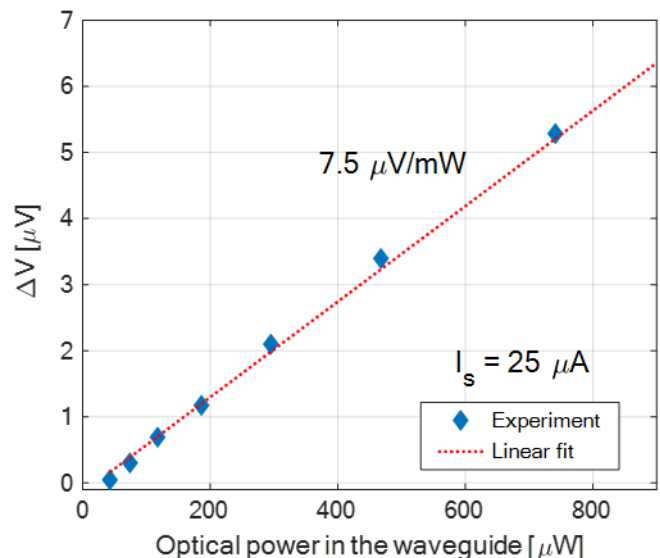e system step response to reach $1 - e^{-1} \approx 63.2\%$ of its final value, is about 1.2 µs which corresponds to a bandwidth of about 132 kHz. The measured response is in very good agreement with simulations (yellow curve) performed by using a time-dependent FEM model, showing a time response of 1.1 µs. The limit to the SPD speed is set by the heat capacity of the dielectrics and the gold's resistivity thermal constant (the electronics response in blue).
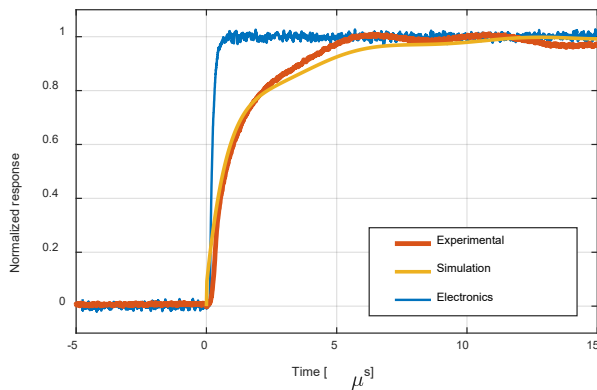

Fig. 14. Normalized time response of the SPD. In blue, the response time of the SPD when electronically and in orange when optically excited. In yellow, the simulated response time.

V.   CONCLUSION

In conclusion, we demonstrated the possibility of monitoring the light intensity in TiO_2 waveguides by exploiting photothermal effect in a multimode SPD. By optimising the geometry of the device, we exploited constructive interference of the SPP modes in order to minimize the coupling loss at the dielectric-plasmonic waveguide interface and optimize the absorption efficiency in the metal. This allows an absorption efficiency, and hence a photothermal response, that is 1.7 times bigger than the value observed for TE propagation, where SPP propagation is inhibited. As a result, the fabricated device, which is extremely compact in size (1.6-µm-long), exhibits a sensitivity (-20 dBm) and a time response (>100 kHz) that fulfils the requirements for implementing monitor and control operations in PICs. The SPD insertion loss, which is about 5 dB in the fabricated devices (2 dB in simulations) can be substantially reduced by introducing a mode adapter at the input/output sections of the plasmonic waveguide [20]. The fabrication process is extremely simple and versatile since it can be ported to any dielectric waveguide platform, where monolithic integration of semiconductor photodetectors is not a viable approach.

VI.   ACKNOWLEDGMENT

VII.   REFERENCES

[1] R. Hui, "Photodetectors," in *Introduction to Fiber-Optic Communications*, Academic Press, 2020, pp. 125-154.

[2] D. F. Logan, P. Velha, M. Sorel, R. M. De La Rue, P. E. Jessop and A. P. Knights, "Monitoring and Tuning Micro-Ring Properties Using," *IEEE PHOTONICS TECHNOLOGY LETTERS,* vol. 24, no. 4, pp. 261-263, 2012.

[3] R. Kingstone, "Optical Detectors," in *Ecncyclopedia of Physical Science and Technology (III Edition)*, Academic Press, 2001, pp. 237-253.

[4] D. F. Logan, P. Velha, M. Sorel, R. M. De La Rue, A. P. Knights and P. E. Jessop, "Defect-Enhanced Silicon-on-Insulator Waveguide Resonant Photodetector With High Sensitivity at 1.55 µm," *IEEE Photonics Technology Letters,* vol. 22, no. 20, pp. 1530-1532, 2010.

[5] F. Morichetti, S. Grillanda, M. Carminati, G. Ferrari, M. Sampietro, M. J. Strain, M. Sorel and A. Melloni, "Non-Invasive On-Chip Light Observation by Contactless Waveguide Conductivity Monitoring," *IEEE Journal of Selected Topics in Quantum Electronics,* vol. 20, no. 4, pp. 292-301, 2014.

[6] J. Homola, "Surface Plasmon Resonance Based Sensors," in *Springer Series on Chemical Sensors and Biosensors*, Springer, 2006.

[7] W. L. Barnes, A. Dereux and T. W. Ebbesen, "Surface plasmon subwavelength optics," *Nature,* no. 424, pp. 824-830, 2003.

[8] K. M. Mayer and J. H. Hafner, "Localized Surface Plasmon Resonance Sensors," *Chemical Reviews,* vol. 6, no. 111, pp. 3828-3857, 2011.

[9] A. Kumar, J. Gosciniak, T. Andersen, L. Markey, A. Dereux and S. Bozhevolnyi, "Power monitoring in dielectric-loaded surface plasmon-polariton waveguides," *Opt. Express,* vol. 18, pp. 12971-12979, 2011.

[10] H. Wu, K. Ma, Y. Shi, L. Wosinski and D. D, "Ultracompact on-chip photothermal power monitor based on silicon hybrid plasmonic waveguides," *Nanophotonics,* vol. 6, no. 5, pp. 1121-1131, 2017.

[11] J. Gosciniak, M. Nielsen, L. Markey, A. Dereux and B. S, "Power monitoring in dielectric-loaded plasmonic waveguides with internal Wheatstone bridges," *Opt. Express,* vol. 21, no. 5, pp. 5300-5308, 2013.

[12] M. M. Mennemanteuil, G. Colas-des-Francs, M. Buret, A. Dasgupta, A. Cuadrado, J. Alda and A. Bouhelier, "Laser-induced thermoelectric effects in electrically biased nanoscale constriction," *Nanophotonics,* vol. 7, no. 12, pp. 1917-1927, 2018.

[13] J.-C. Weeber, K. Hassan, A. Bouhelier, G. Colas des Francs, J. Arocas, L. Markey and A. Dereux, "Thermoelectric detection of waveguided surface plasmon propagation," *Applied Physics Letters - APPL PHYS LETT,* vol. 99, 2011.

[14] P. Debackere, S. Scheerlinck, B. P and B. R, "Surface Plasmon Interferometer in Silicon-on-Insulator: Novel Concept for an Integrated Biosensor," *Opt. Express,* vol. 14, no. 16, pp. 7063-7072, 2006.

[15] S. Mirzanejhad, A. Ghadi and M. Daraei, "Numerical study of nanoscale biosensor based on surface plasmon polariton propagation in Mach-Zehnder interferometer structure," *Physica B: Condensed Matter,* vol. 557, 2018.

[16] H. A. Okda, S. I. Rabia and H. M. H. Shalaby, "Sensitivity enhancement of a difference interferometer refractive index sensor based on a silicon-on-insulator hybrid plasmonic waveguide," *Journal of the Optical Society of America B,* vol. 38, no. 4, pp. 1405-1415, 2021.

[17] P. Berini, "Plasmon-polariton waves guided by thin lossy metal films of finite width: Bound modes of asymmetric structures," *Phys. Rev. B,* vol. 61, no. 15, pp. 10484-10503, 2000.

[18] A. Andrieux, M. M. Mennemaneuil, N. Geoffroy, M. Emo, L. Markey and K. Hammani, "Optimized ICPCVD-based TiO2 photonics," *Materials,* vol. 15, p. 2578, 2022.

[19] F. Morichetti, A. Canciamilla, C. Ferrari, M. Torregiani, A. Melloni and M. M, "Roughness Induced Backscattering in Optical Silicon Waveguides," *Phys. Rev. Lett,* vol. 104, no. 3, 2010.

[20] P. Shi, G. Zhou and F. S. Chau, "Enhanced coupling efficiency between dielectric and hybrid plasmonic waveguides," *J. Opt. Soc. Am. B,* vol. 30, no. 6, pp. 1426-1431, 2013.

Andres Martinez (1997) achieved the M.Sc. at Politecnico di Milano in Telecommunication Engineering with a thesis on plasmonic photodetectors. In March 2022 he started to work as a researcher at the Photonic Devices Group of Politecnico di Milano. His work is mainly focused on plasmonic detectors and PICs for free space optics applications. He is currently working on EU project NEBULA and a project between Politecnico and Huawei.

Vittorio Grimaldi (1994) received both his bachelor's and master's degree (cum laude) in electronics engineering from Politecnico di Milano in 2016 and 2019, respectively. He is currently a PhD student in the Department of Electronics, Information and Bioengineering of Politecnico di Milano. He is currently working on the development of sensors, actuators and algorithms for thermal stabilization and real-time control in plasmonic platforms.

Christian de Vita Christian (1995) achieved the M.Sc. at Politecnico di Milano in Telecommunication Engineering with a thesis on Silicon oxycarbide for integrated Photonics. In November '19 he started the Ph.D. in Information Engineering with a scholarship focused on multilayer thin films for UV to LWIR operation. His work is mainly focused on the sensing of the light with invasive and non-invasive techniques, consisting in the simulations, fabrication and testing of devices realized on different platforms and different wavelengths depending on their applications. He is currently working on EU projects Superpixels and Nebula, and in the context of the JRC between Politecnico and STMicroelectronics.

Deepak K Sharma received his Ph.D. in Physics from the Indian Institute of Science Education and Research, Pune, India in 2020. Afterward, he was a postdoctoral research fellow at Laboratoire Interdisciplinaire Carnot de Bourgogne UMR 6303 CNRS/Université de Bourgogne, France during the years 2020-2021. Currently, he is working as a Scientist at Agency for Science, Technology, and Research (A*STAR), Singapore. His research interests comprise plasmonics with specific emphasis on spin-orbit interactions and nonlinear effects, integrated photonics, and metasurface for flat lenses and integrated devices.

Isabelle Gallet (Engineer, CNRS Female). Diploma of Higher Education in Physical Measurement (1998 University Institut of Technology of Montbéliard, Fr). Trained internally in various laboratoies (LURE and ICMMO in Paris, ICBDijon), she is specialized in e-beam and UV lithography, plasma etching, characterization of materials.

Dr. Aurore Andrieux (IE, CNRS). PhD Materials Science (2015 - Uni. Lorraine, FR). She developed processes based on plasma-assisted thermochemical treatments to harden up and pattern steel surfaces at micrometer scale during her PhD (ANR project MicroGaMe). She specialized then in nanotechnologies, as a member of the thin film deposition Unit in the technology center MIMENTO of the Femto-ST Institute (Besançon, FR) before entering the CNRS in December 2018 as engineer in the field of Thin film deposition and Nanofabrication. She is currently part of the Nanofabrication team in the technological platform ARCEN-CARNOT of the ICB Laboratory (Dijon, FR), as responsible of plasma-assisted Chemical Vapor Deposition, ion-assisted e-beam evaporation and chemical-mechanical polishing tools. She is focusing in oxide and nitride thin films deposition and characterization.

Juan-Miguel AROCAS GARCIA is an engineer at CNRS (Centre National de la Recherche Scientifique) with 20 years of experience, specialized in thin film deposition (e-gun/thermal evaporation, sputtering), developing new materials (TiO_2, TiN, Ta_2O_5…). He is responsible for the deposition machines in the centre of nanofabrication at Université de Bourgogne. He also characterizes the deposited materials by ellipsometry, XRD and XPS. He has worked in different European projects for plasmonic and integrated photonics applications.

Ass. Prof. Kamal Hammani received the PhD degree at the University of Burgundy in 2011. During 2012-2013, he worked as a post-doctoral research fellow at the Optoelectronics Research Center (University of Southampton) in United-Kingdom. Since September 2013, he is an assistant professor at the University of Burgundy. His Research (at Laboratoire Interdisciplinaire Carnot de Bourgogne UMR 6303 CNRS/uB) covers nonlinear optics, optical communications, optical fibers, frequency-comb, nanophotonics and plasmonics for applications in opto-electronics in near- and mid- infrared

Dr. Laurent Markey. PhD in Materials Sciences (1998 - Uni. Lille, FR). He is a research engineer at CNRS (Centre National de la Recherche Scientifique) managing the nano-micro-fabrication facilities at Université de Bourgogne (Dijon, FR). He has strong experience in nanotechnology and materials science, more specifically in lithography, functionalization and nanofabrication processes applied to photonics and microfluidics and biosensors. He has been involved in different EC-funded projects, has more than 17 years of scientific contribution in the fields of nanophotonics, plasmonics, nano-bio-sensors and is co-author of more than 70 peer-reviewed papers.

Prof. Jean-Claude Weeber received his PhD from the University of Burgundy (uB) in 1996 in Dijon. He is full-time professor at uB since 2005. His main fields of interest are plasmonics for datacom and sensing. He is currently involved in projects targeting disruptive integrated optics approaches for neuromorphic network applications.

Dr. Alexandre Bouhelier. PhD Physics (2001-Uni. Basel, CH). His research started with the development of optical near-field and scanning probe microscopy. He spent four years in the US as a postdoc before integrating the CNRS where is now a research director working at Laboratoire Interdisciplinaire Carnot de Bourgogne Université de Bourgogne, Dijon, France. His current research directions are (i) focused at developing atomic-scale electro-optical functional components and (ii) understanding/controlling nonlinear plasmonics in photonic integrated chips.

Marco Sampietro (Member IEEE), born in 1957, is full professor of Electronic Circuits and Devices at Politecnico of Milano, Italy. He is co-author of more than 220 peer-reviewed international publications and holds 5 patents. He has been the coordinator of many national and international research projects and scientific partner in seven large-size European projects within the FP6, FP7 and HORIZON2020 (STREAMS, NEBULA). He is responsible for the activities in high-sensitivity instrumentation for the nanoscience, with a focus on the design of electronic integrated circuits for monitoring, tracking and feedback controlling the working point of optical micro-integrated devices and has coordinated the activity on the electronic system platform to exploit photonic probes on complex photonic architectures. From 2012 to 2018, he was the Dean of the Bachelor's and Master's Course Program in Electronics Engineering at Politecnico di Milano.

Andrea Melloni OSA Fellow, he is Full Professor at Dipartimento di Elettronica, Informazione e Bioingegneria – Politecnico di Milano – where he leads the group of Photonic Devices and teaches the master course "Photonics Devices". With a background in microwaves, his field of research is in the analysis, design, characterization and exploitation of passive integrated optical devices for telecom and sensing. He has been one of the pioneers of the slow light concept and its exploitation in the linear and nonlinear domain. He is currently contributing to define the new schemes of generic photonic foundries in Europe. In 2008 he founded the company Filarete, for the development and commercialization of the first circuit simulator for integrated optical circuits, ASPIC (www.aspicdesign.com). He holds 13 international patents in the field of integrated optics and components and he is author and co-author of over 90 publications on the major international journals.

Francesco Morichetti (MSc 2001, PhD 2008) is Associate Professor at Politecnico di Milano and Head of the Photonics Devices Lab of Politecnico di Milano. His main interests are in optical devices and photonic integrated circuits for applications in the field of optical communications, interconnects and sensing. Recent research activity is focused on programmable photonic circuits and the development of automated control and calibration techniques for reconfigurable optics. He has been involved with leading roles in several EU Projects (FP6, FP7, H2020). He is author/coauthor of 3 chapters of international books, 90 peer-reviewed publications in international journals, more than 200 publications on proceedings of international conferences, and 10 international patents in the field of integrated optics. Since 2010 he has been a member of the scientific panel of Spotlight on Optics (Optica).